

RSC Advances



This is an *Accepted Manuscript*, which has been through the Royal Society of Chemistry peer review process and has been accepted for publication.

Accepted Manuscripts are published online shortly after acceptance, before technical editing, formatting and proof reading. Using this free service, authors can make their results available to the community, in citable form, before we publish the edited article. This *Accepted Manuscript* will be replaced by the edited, formatted and paginated article as soon as this is available.

You can find more information about *Accepted Manuscripts* in the [Information for Authors](#).

Please note that technical editing may introduce minor changes to the text and/or graphics, which may alter content. The journal's standard [Terms & Conditions](#) and the [Ethical guidelines](#) still apply. In no event shall the Royal Society of Chemistry be held responsible for any errors or omissions in this *Accepted Manuscript* or any consequences arising from the use of any information it contains.

ARTICLE

Quantitative Structure-Property Relationship Modeling of Ruthenium Sensitizers for Solar Cells Applications: Novel Tools for Designing Promising Candidates.

Cite this: DOI: 10.1039/x0xx00000x

Received 00th January 2012,

Accepted 00th January 2012

DOI: 10.1039/x0xx00000x

www.rsc.org/

Sara Tortorella,^a Gabriele Marotta,^b Gabriele Cruciani,^{a,*} Filippo De Angelis^{b,*}

To date, the most diffused way of screening new potential sensitizers for dye sensitized solar cells is via the traditional time and money consuming trial and error approach.

In this study we explore the possibility of extending drug discovery and cheminformatic approaches to the field of material science with the aim of a quantitative structure-property relationship elucidation that could lead to a fast and inexpensive in silico screening of new ruthenium sensitizers for third generation solar cells.

Starting from the building of a database of already tested candidates used to train the predictive models, appropriate descriptors extracted from images of 3D molecular interaction fields (GRID/MIFs), as well as semi-empirical calculated descriptors, were chosen to describe the target structures. Then, structure-performance (J_{sc} , V_{oc} and PCE) models were built and analysed in order to elucidate structure-property relationships and interesting results were obtained.

In particular, we were able to find the molecular descriptors that more contribute to enhance the performance investigated, thus finding directives for the design of potentially high-performing candidates. We also proposed an efficient correction of the experimental J_{sc} and V_{oc} based on the quantity of the LiI additive for electrolyte used to build the devices.

In the early stage of this project, we demonstrated that molecular modelling methods could be successfully extended to the field of material science as alternative to the traditional expensive and time-consuming trial and error approach.

Introduction

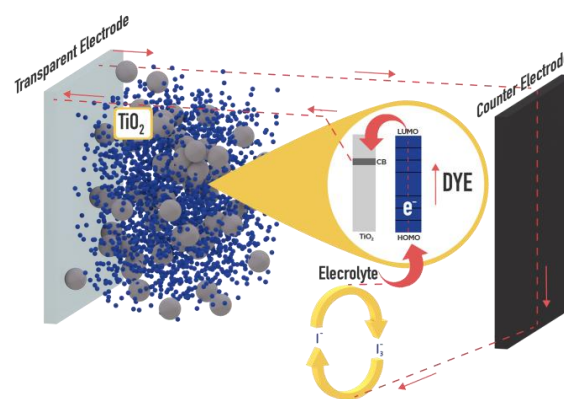
Research on renewable energies has become a key issue for a sustainable development.

The increasing interest in the solar energy market has led to various generations of photovoltaic technologies.^{1,2} The latest technology, so called third generation, includes, among others, the dye-sensitized solar cell (DSSC). DSSCs appear as one of the most promising technologies due to their low-cost, large-scale production (e.g. roll-to-roll, inkjet printing) and the appealing potential of merging the extreme versatility of thin film technology with the electronic features needed for the solar cell operation.³⁻⁵ To this end, research is moving forward to solve the issue related to their relatively still low efficiencies and limited lifetime, if compared with the traditional silicon-based solar cells.

In DSSCs the light-to-electricity conversion is determined by a dye sensitizer, either an organic or metallorganic molecule, which absorbs the solar radiation and transfers the photoexcited electron to a wide band gap semiconductor electrode consisting of a TiO_2 network composed of nanometer-sized particles, while the concomitant hole is transferred to the redox electrolyte to generate carriers transport to the electrodes as shown in Scheme 1.⁶ The

overall conversion efficiency (η) of the DSSC is determined by the short circuit current (J_{sc} , mA/cm^2), the open circuit potential (V_{oc} , V), the fill factor (FF, adimensional parameter), and the power of the incident light (P_i , mW/cm^2), namely:

$$\eta = (V_{oc} \times J_{sc} \times FF) / P_i \quad (1)$$



Scheme 1. Operational principle of a DSSC based on I^-/I_3^- redox shuttle.

It is well known that η markedly depends on the electronic and optical properties of the dye sensitizer. The dye is responsible for the light harvesting step and plays a crucial role in many of the key electron transfer processes occurring at the TiO₂/dye/electrolyte interface.^{7,8} Therefore, by a rational design of the dye sensitizer we can tune its absorbing properties and control the electron transfer processes that ultimately would lead to optimization of the solar cell efficiency.

The sensitizer which had a key role in significantly advancing the DSSC technology was Ruthenium (II) tetraprotonated[*cis*-(dithiocyanato)-Ru-bis(2,2'-bipyridine-4,4'-di-carboxylate)] complex (N3).⁹ Then, similar dye sensitizers with different ligands on the pyridine moiety anchoring the dyes on the surface of the TiO₂ nanoparticles have been proposed in order to elucidate structure-properties relationships and to achieve higher conversion efficiencies.¹⁰⁻¹³

In this context, approaches that involve totally *in silico* screening of potential candidates could encourage researchers to substitute the traditional slow and expensive *trial-and-error* approach with a rational design of high-efficiency materials. Strategies combining computational chemistry methods (e.g. *ab initio* and semiempirical calculations) have already been explored to identify high performing materials for solar cells.¹⁴⁻¹⁷ However, because of the complexity of the overall solar cell operation, these methods cannot straightforwardly predict relevant solar cell properties such as the final efficiency (η) in terms of molecular structure-properties relationships.

An alternative approach could be the use of chemometric tools to elucidate quantitative structure-property relationships (QSPR) and to build models that establish a mathematical relationship between a set of molecular descriptors characterizing the target molecule and a property of interest.¹⁸ This approach is, for instance, currently and successfully employed in the drug design field¹⁹⁻²¹ and other statistical approaches have recently been used to rationalize experimental data and to optimize the fabrication process of Grätzel solar cells.^{22, 23, 24}

We propose in this study an innovative approach of extending the molecular modelling and drug design techniques to the photovoltaic material research field. By exploiting an existing data-set of photovoltaic efficiencies for ruthenium-based dyes, we find that combining calculated semiempirical descriptors (HOMO, LUMO, bandgap), chosen descriptors extracted from images of 3D molecular interaction fields (GRID/MIFs) and 2D structural descriptors also used in drug design we can have an exhaustive and target-oriented description of the dye molecule of interest and a Partial Least Squares PLS models can be built to both rationalize experimental data and to predict new compounds photovoltaic performance.

Methodology

For the purpose of efficiently describing entire dataset of molecules, we used VolSurf+, a completely automated procedure to convert 3D molecular fields into physicochemical relevant molecular descriptors that are computationally efficient and well suited for fast quantitative structure-property relationship studies.^{25, 26} The basic concept of VolSurf+ is to extract the information present in 3D molecular field maps into few quantitative numerical descriptors that are easy to understand and to interpret. VolSurf+ provides a set of 135 descriptors that are relevant for drug design applications, but some of them nonetheless can be useful in the description of OPV donor materials (Figure 2).²⁷ In particular, the VolSurf+ chosen descriptors were (ESI 1.1):

1. Structural descriptors: molecular weight, molecular volume, molecular surface, rugosity, molecular

globularity, flexibility parameters, number of charged centers

2. Hydrophilic/hydrophobic and H-bond donor/acceptor regions descriptors: hydrophilic/hydrophobic volumes, capacity factors, interaction energy moments, polar and hydrophobic surface areas, H-bond donor/acceptor volumes, polarizability and dispersion forces
3. Mixed descriptors: critical packing, diffusivity, LogP octanol/water and cyclohexane/water, percentage of unionised species at different pH

As a fourth set of descriptors, we introduced electronic properties descriptors: the HOMO, LUMO, HOMO-LUMO gap and the molecular electrostatic potential. The electronic properties were computed by semiempirical methods with the Gaussian09 package.²⁸ To find the best compromise between reliability of results and time of computing, we screened different DFT models chemistry for geometry optimization (B3LYP,^{29, 30} AM1³¹) and for excited states TDDFT calculation (B3LYP, MPW1K³², ZINDO³³) and we chose the combination of semiempirical AM1 for ground-state geometries optimization and ZINDO for excitation energies calculation.

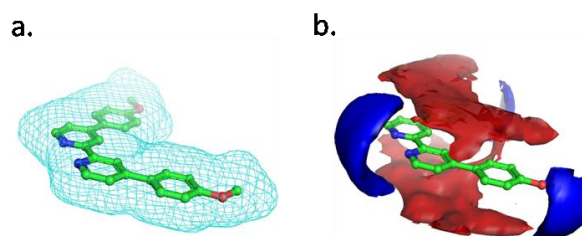


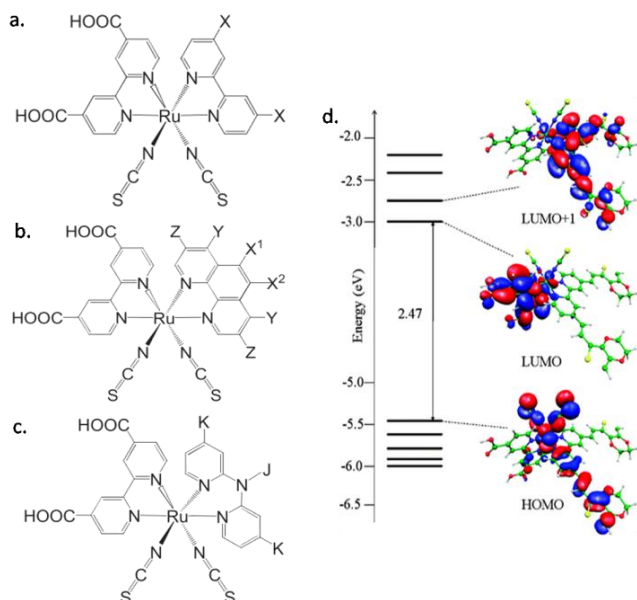
Figure 2. Example of a) shape and b) hydrophobic (red) and hydrophilic (blue) molecular interaction fields (MIFs) for ligand 11.

Combining such semi-empirical calculated descriptors, models predicting structure-photovoltaic property relationships (open circuit voltage, current intensity or power conversion efficiency) have been built. Considering the database of already tested ruthenium sensitizers collected by Yin et al,³⁴ a subset of 73 dyes able to include significant structural and performance variation (the *training set*, ESI 1.2) was chosen. The dyes mentioned in the paper are referred to with the same label used in ref. 33 and are reported in Table 1. Then, Partial Least Squares algorithm³⁵ from the VolSurf+ package has been used to find the best molecular descriptors correlation with different performances of interest. The correlation coefficient R² (amount of performance “explained”, ranging from 0 to 1) and the cross validated correlation coefficient Q² (amount of performance “predicted”, ranging from 0 to 1) were then used to analyse the goodness and reliability of the obtained models. Weights plot (see e.g. Figure 5) have been used to elucidate structure-property relationships as well as descriptors-performances correlations and interpreted in term of descriptors positioning (blue dots) in respect to the axis origin and the performance (yellow dot): descriptors important for the nth latent variable fall far from the origin along the nth axis in the plot, and descriptors more related to the performance lay near the performance itself (directly correlated) or in its symmetric to the origin space (inversely correlated).³⁶ Descriptors/performances correlation was also explicated by reporting the Variables Importance on PLS (VIPs).³⁷

Results and Discussion

We applied the cheminformatic approach described above to build structure-property relationships models for a series of ruthenium sensitizers effectively employed in DSSCs. Various bipyridine-based ligands were chosen to define a *training set* of 73 heteroleptic ruthenium dyes (see methodology). The ruthenium scaffold is unchanged for all the molecules of the training set and only the 4,4'-dicarboxylic acid-2,2'-bipyridine (dc bpy, Figure 3a)- or 1,10-phenanthroline (1,10- phen, Figure 3b)- or dipyriddyamine (DPA, Figure 3c)-based ancillary ligands are systematically substituted.

Figure 3. Molecular structures of investigated ruthenium photosensitizers with



various a) bipyridine- b) phenanthroline- and c) dipyriddyamine-based ancillary ligands; example of electronic structure of investigated electronic scaffold

Selected VolSurf+ molecular descriptors were used to describe the selected structures (see methodology). However, electronic properties cannot be neglected when considering this class of materials because it is well known that the HOMO, but in particular LUMO (Figure 3d), positioning can dramatically affect the electron injection step.³⁸ Therefore, we added three semiempirical calculated descriptors (geometry optimization with AM1 followed by excited states calculation with ZINDO) in order to evaluate the HOMO, the LUMO and the bandgap.

Experimental J_{sc} , V_{oc} and PCE were simultaneously modelled with the PLS algorithm. The first step of the obtained model analysis was to look for evident outliers, because the presence of outliers generally means that some molecular descriptors are missing to properly catch their structure-property relationship, or that experimental data contain alteration in respect to the rest of the database. Two strong outliers (dye 60 and 63) could be detected on the bottom left part of the predicted/versus experimental plot for the PCE model on the whole training set (Figure 4a). To figure out why the model is unable to correctly catch structure-properties relationships for the outliers we looked at the dye structures and considered them with respect of the entire training set.

Ligands 60 and 63 belong to the same family of dyes 61 and 62: they all have at least one $-NO_2$ or $-NH_2$ on the 1,10-phenanthroline-based

ancillary moiety (Table 1 B) and they show the lowest performance of the series. It is known that $-NH_2$ groups on the dye structure lead to a decreasing of all the performances with respect to the same dye without this substituent.³⁹ At the same time, the $-NO_2$ moiety leads to a quenching of fluorescence in organometallic complexes, thus competing with charge injection and decreasing the solar cell operation.⁴⁰ Our model succeeds in reproducing the performance trend and, even if overestimated in case of dyes 60 and 63, predict their performances as the lowest of the series. Indeed, despite the fact that the two moieties are very different from a chemical point of view, they are projected in the same chemical space which means that our model have found as detrimental to the performance the presence of both $-NO_2$ or $-NH_2$ as it actually is.

A second group of outliers could be identified in dye 6 and 65 (Figure 4a).

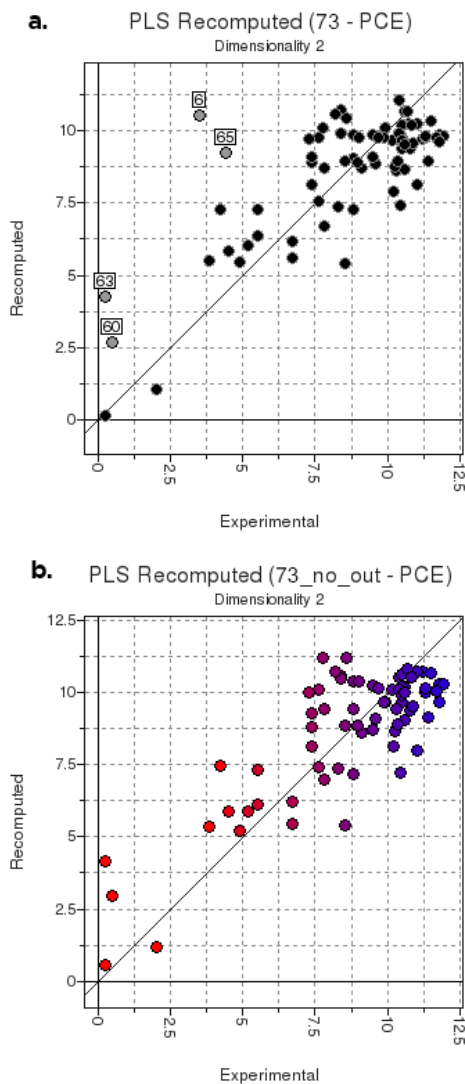


Figure 4. Predicted versus Experimental plot for PCE model for a) the whole training set and b) after the outliers exclusion (6, 65), coloured by PCE value: red-low PCE, blue-high PCE

ARTICLE

Table 1 Substituents fragments of the mentioned dyes, Ref. 33

A: 4,4'-dicarboxylic acid-2,2'-bipyridine scaffold			
1	•-H	2	•-CH ₃
3	•-C ₆ H ₁₃	4	•-C ₉ H ₁₉
5	•-C ₁₃ H ₂₇	6	•-C ₁₈ H ₃₇
23		25	•-O-R _f R _f = C ₂ F ₄ H
26	•-O-R _f R _f = C ₃ F ₇	27	•-O-R _f R _f = C ₄ F ₈ H
30		32	
39		46	
53		54	
56			
B: 1,10-phenantroline scaffold			
60	X ¹ =H, X ² =NH ₂ , Y=Z=H	61	X ¹ =X ² =NH ₂ , Y=Z=H
62	X ¹ =H, X ² =NO ₂ , Y=Z=H	63	X ¹ =X ² =NO ₂ , Y=Z=H
64	X=Y=H Z= 	65	X=Y=H Z=

Ligand 6 differs from the analogues 1, 2, 3, 4, 5 for the alkyl chain length (Table 1 A). Usually long alkyl chains on the dbpy ligand function as an electrical insulating barrier layer between the sensitizer dye and the hole-transporting medium, thereby reducing interfacial charge recombination losses and increasing the open circuit potential (V_{oc}) and short-circuit photocurrent (J_{sc}). As the PCE is increasing when elongating the chain length for dye 1, 2, 3, 4, 5, the linear regression algorithm used takes this feature as important for the PCE enhancement. However, dye 6 deviates from this trend because of the observed slower charge recombination between the electrolyte and the injected electron⁴¹ and the inhomogeneous dye-loading on the TiO₂ surface due to the folding of the long C18 chains reducing the recombination blocking effect of the alkyl chain spacer.⁴² In dye 65 (CYC-P2), as in the correctly

estimated 64 (CYC-P1, Table 1 B), the ancillary ligand is an alkylthiophene and they only differ for the conjugation length. In the more conjugated CYC-P2 the HOMO is localized on the ligand-P2, resulting in a weak oscillator strength of the MLCT transition that could be the major reason for its low cell efficiency.

All these considerations reveal why elongating the conjugation length of the ligand is not a must for improving the conversion efficiency of the ruthenium.⁴³ Indeed, all the evident outliers are overestimated because compared with the analogues in the training set, but it is reasonable to understand that a simple linear regression model could not catch cut-off and non-linear structure-property relationships. Therefore, we decided to exclude only the second two outliers from the training set, those related to clearly non linear structure-properties relationships. By excluding these molecules from the training set, both R² and Q² statistical parameters, thus the

overall predictive ability, increase: the starting model for PCE showed, with two latent variables, R^2 and Q^2 value of 0.58 and 0.44, respectively (Figure 4a). By excluding the outliers these values increase to 0.67 and 0.56, respectively (Figure 4b and Table 2). The good R^2 and Q^2 values of the model indicate that we should be able to predict with confidence the performance of novel candidates: for instance, considering those among the best performing materials, dye 32 (oligophenylenevinylene based, Table 1 A) is recalculated at a PCE of 11.2% as actually is, dyes 39 and 46 (hexylthio-terminal chain on the dbpy, Table 1 A) are recomputed to be 11.0% and 10.0% when they are 11.5% and 11.2% PCE, respectively.

In order to elucidate relationships within the investigated performances and in respect to the molecular descriptors to identify directives for the design of novel candidates, we interpreted the weights plot of the model. The first observation which can be noted is the almost complete overlap between the J_{sc} and the PCE data set, which means that molecular features important for an increase in J_{sc} play a more important role than those for the V_{oc} to increase the PCE. However, the V_{oc} values do not lay distant, so we can define parameters that could simultaneously improve J_{sc} and V_{oc} , thus the final PCE. In particular, among the most inversely correlated descriptors we find the USR 6 (which accounts for the presence of NO_2 and NH_2), PHSAR/PSAR (considering the ratio between the polar surface area and the hydrophobic surface area and the ratio between the polar surface area and the surface, respectively) and WO4 and WO5 (H-bond donor volumes), while among the most directly correlated we found LogPn-oct and LogPc-Hex (the logarithm of the partition coefficient between 1-octanol and water and cyclohexane and water), LgD5/LgD10 (accounting for the LogP at different pH), G (globularity) and FLEX_RB (the ratio between flexibility and the number of rotatable bonds).

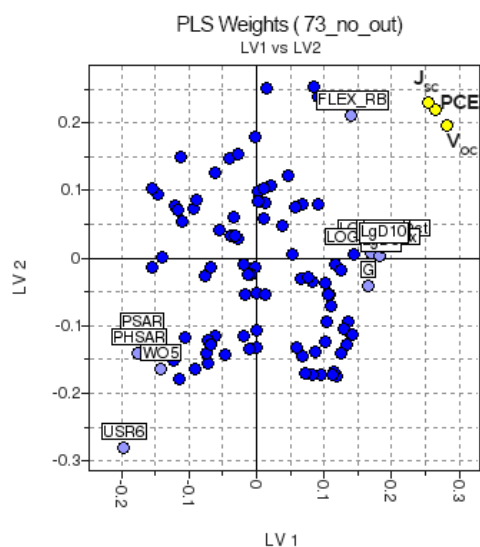


Figure 3. Weights plot of the model after the outlier exclusion

These findings indicate that promising candidates should not have NO_2 and NH_2 moieties, as expected; they should have small polar regions or polar regions balanced with hydrophobic regions and not have wide molecular regions able to generate attractive H-donor interactions. At the same time, they should be hydrophobic and possibly have a certain extent of globularity and flexibility but avoiding too many rotational bonds. Although these indications may seem difficult to understand, the advantage in using the employed molecular field interaction (MIF)-based descriptors is that they are

immediately calculated as soon as we design the molecule of interest so that we can easily visualize and verify the previously suggested directives. Moreover, by projecting new candidates on the proposed models, a quick estimation on their performance can be obtained. For instance, a straightforward way to use this model is by plotting the LV1/LV2 plot, colour it by the performance value and colour the object by their performance value (Figure 6a). New candidates can then be projected on this plot and the performance directly estimated from their positioning: if the projections lay on the blue area, they will be promising sensitizers and worth synthesizing and testing. Moreover, a cluster in the LV1/LV2 plot indicates that similar features associated with the modelled performance have been found in the dyes that are therefore grouped together. It is interesting to note that clear clusters can be identified on the obtained LV1/LV2 plot: dyes 25, 26, 27 are the only containing hydrophobic fluorine chains which allow these dyes to adsorb on the TiO_2 surface more strongly and provide higher dye density than alkyl chains, and 23 contains with Li^+ -coordinating oxyethylene side chains (Table 1 A); sensitizers 60-63, as already pointed out, contain at least one NO_2 or NH_2 ; 53, 54, 56 contain carbazole substituted thiophene moieties and 30 and 32 both contain oligophenylenevinylene groups as an ancillary ligand (Table 1 A) and all have a PCE in the range of 9-11% (Figure 6b). The great advantage in using cheminformatic tools is that sometimes these feature-associations would not have been deducible only by looking at the structure. Therefore, when looking for new sensitizers and to gain insights into uncovered structure-property relationship we would save time and money by finding candidates that lay on the not-yet-explored chemical space.

Modelling of the Effect of Li^+ ions

Inspired by the known effect of the LiI electrolyte additive on the electric properties of the device, we also investigated this effect in modeling our target experimental data. In particular, it is known that by adding LiI, the V_{oc} tends to decrease while the J_{sc} increases due to a down-shift of the TiO_2 conduction band and induced shortest lifetime.^{44, 45}

Considering what has already been observed experimentally on the entity of this effect, we suggest two corrections for the values of J_{sc} and V_{oc} as:

$$J_{sc} = J_{[Li]} \cdot (1 + \text{Log}[LiI]) \quad (2)$$

$$V_{oc} = V_{[Li]} + 0.05 \times (1/p[LiI] - 1) \quad (3)$$

where $[LiI]$ is the molar concentration of the LiI used to build the tested device and $J_{[Li]}$ and $V_{[Li]}$ are the measured short circuit current and open circuit voltage, respectively.

By applying the proposed correction to both J_{sc} and V_{oc} on the subset of the 54 dyes for which the LiI additive concentration used to build the solar device have also been reported (ESI 1.2), we obtain models that show an improved correlation and successfully predict the trend of the investigated performances, confirming either the reliability of the proposed correction and the understanding of structure-property relationships by the model (Figure 7). In particular, the models obtained by applying these considerations show R^2 and Q^2 values of 0.75 and 0.66 when correcting J_{sc} for the LiI effect, which further improve to 0.79 and 0.64 for V_{oc} considering two latent variable (Table 2, LiI corrected). In order to investigate the single performance contribution we then separated and analysed the coefficient of the linear regression model. In Figure 8 we reported the coefficient of the linear regression with an absolute value higher than 0.3 for every performance.

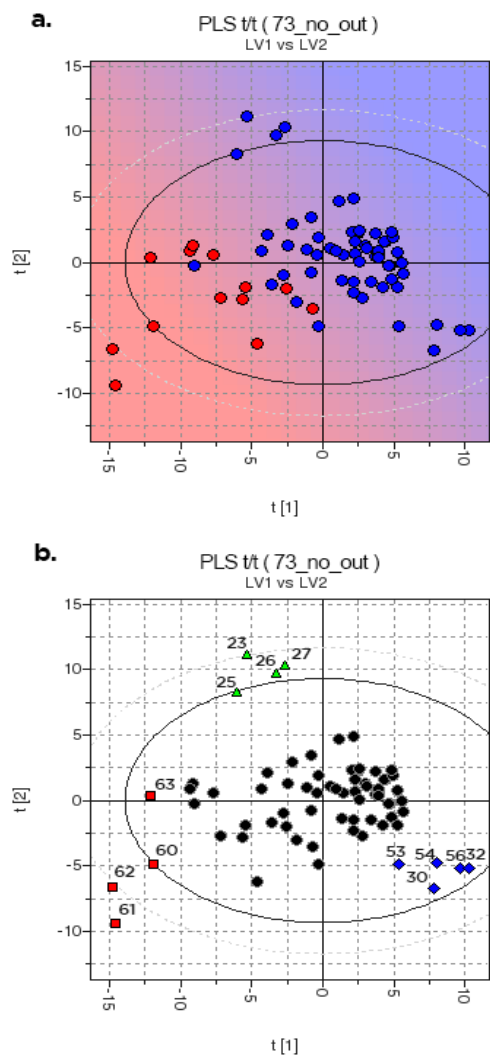


Figure 4. LV1/LV2 plots for the 73_no_out model, a) background coloured by PCE (from red-low PCE- to blu-high PCE) and compounds by experimental PCE value: red PCE < 7, blu PCE > 7 and b) with clusters highlighted.

For J_{sc} , the more negative coefficients are referred to descriptors of the presence of NH_2/NO_2 , polar surface area, percentage of unionised species is calculated at pH 4 and H-bond donor volumes calculated at different energies (USR6, PSAR/PHSAR, %FU4, WO1-WO6, Figure 8a). At the same time the more positive coefficients belong to descriptors of flexibility/rotatable bond ratio, partition coefficient cyclohexane/water and unbalance between the centre of mass of a molecule and the barycentre of the hydrophobic/hydrophilic regions (FLEX_RB, Log-P c-Hex, ID/IW).

The PCE weights plot shows very similar correlation to J_{sc} : the only difference is that in the PCE the Log-P c-Hex descriptor plays a more important role. Also V_{oc} shows similar correlation but with higher coefficient. It is worth noting that among the directly correlated descriptors, the calculated LUMO (USR2), more than the HOMO (USR1), plays a crucial role (Figure 8b), in fact having the highest positive contribution to the definition of the second latent variable. This is an important statement because, in agreement to what has already been reported, an increase of the LUMO energy of the sensitizers would increase the V_{oc} , while the HOMO plays a less significant role.⁴⁶ This last analysis reveals as important the same molecular descriptors discussed for the not [LiI]-corrected model, confirming the reliability of the already given design rules.

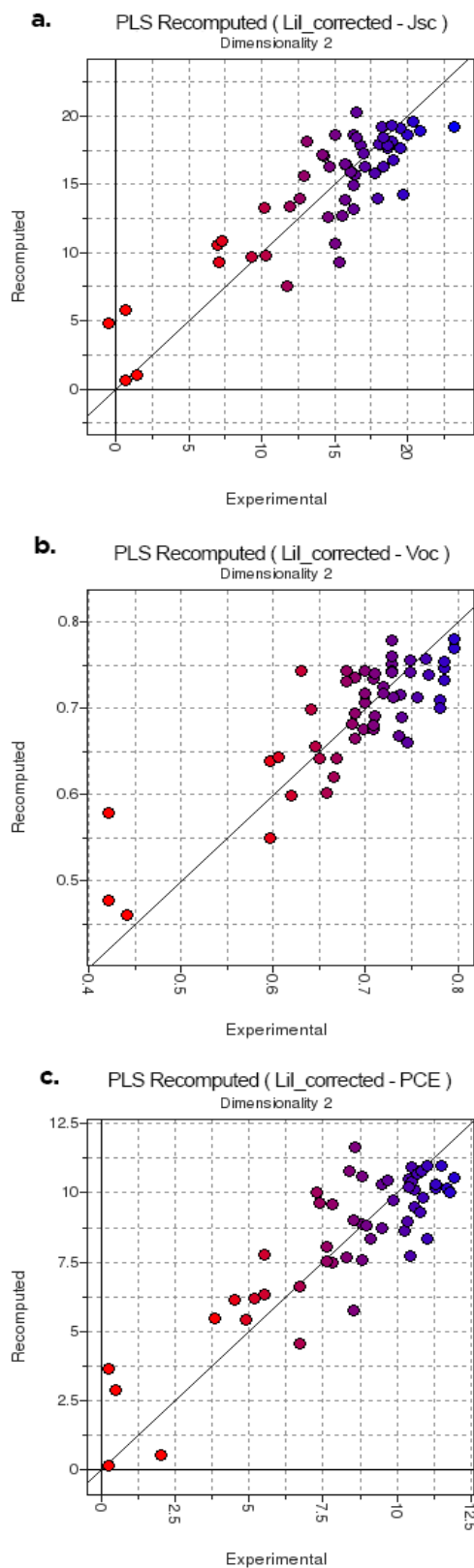
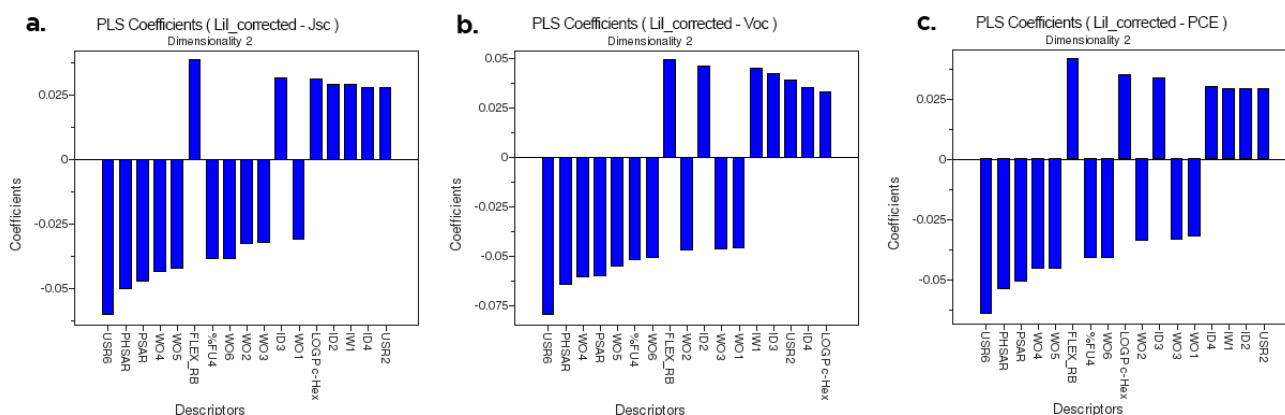


Figure 5. Experimental/Recomputed plot for a) J_{sc} , b) V_{oc} and c) PCE models corrected for the LiI concentration.

Table 2. PLS models performances on the initial dataset (73), after outliers exclusion (73 no out.) and after the proposed J_{sc} and V_{oc} correction (LiI corrected).

Performance Modelled	73		73 no out.		LiI corrected	
	R ²	Q ²	R ²	Q ²	R ²	Q ²
J_{sc}	0.59 ^b	0.41 ^b	0.68 ^b	0.55 ^b	0.75 ^a	0.66 ^a
V_{oc}	0.54 ^b	0.38 ^b	0.56 ^b	0.43 ^b	0.79 ^b	0.64 ^b
PCE	0.58 ^a	0.44 ^a	0.69 ^a	0.59 ^a	0.75 ^a	0.60 ^a

^aModels built with two latent variables^bModels built with three latent variables**Figure 8.** Coefficients for a) J_{sc} , b) V_{oc} and c) PCE models corrected for the LiI concentration.

Conclusions

In this work we demonstrated that cheminformatic and molecular modelling techniques, successfully applied in drug design, could be in principle extended to the material design field.

This first attempt was focused on elucidating structure-property relationships on an extensively experimentally investigated class of ruthenium sensitizers for Grätzel third generation solar cells.

A combination of semi-empirical calculated, 2D structural descriptors and descriptors extracted from images of 3D molecular interaction fields (GRID/MIFs) have been used to describe the dyes. Then, cheminformatic algorithm PLS (Partial Least Squares) has been used to build structure- J_{sc} / V_{oc} -PCE models to find directives for designing promising candidates.

Moreover, for a subset of dyes we proposed a correction of the J_{sc} and V_{oc} based on the quantity of the LiI additive for electrolyte used to build the device.

The obtained models correctly predict the trend of performance for the training set and show encouraging value of R² and Q², therefore could be easily and quickly used to project new candidates as well as big database of molecules to have an estimation of the expected photovoltaic performances.

The goal of this totally *in silico* and high throughput approach is to offer novel instruments to both overcome the traditional *trial-and-error* approach and to look differently into experimental data by means of statistical and molecular modeling tools.

Notes and references

^a Drug Design and Molecular Modeling Laboratory, Department of Chemistry, Biology and Biotechnology, University of Perugia, Italy

^b Computational Laboratory for Hybrid/Organic Photovoltaics (CLHYO), Institute of Molecular Science and Technologies (ISTM-CNR), Via Elce di Sotto 8, I-06123, Perugia, Italy.

- P. C. Choubey, A. Oudhia, R. Dewangan and V. Y. T. P. G. Autonomous, *Recent Res. Sci. Technol.* 2012, 2012, **4**, 99–101.
- K. R. Catchpole and M. A. Green, *Optoelectronic and Microelectronic Materials and Devices, 2002 Conference on*, IEEE, 2002, pp. 59–64.
- M. Grätzel, *J. Photochem. Photobiol. C Photochem. Rev.*, 2003, **4**, 145–153.
- M. Pagliaro, R. Ciriminna and G. Palmisano, *ChemSusChem*, 2008, **1**, 880–891.
- M. Grätzel, *Nature*, 2001, **414**, 338–344.
- A. Hagfeldt, G. Boschloo, L. Sun, L. Klöö and H. Pettersson, *Chem. Rev.*, 2010, **110**, 6595–6663.
- J. N. Clifford, E. Martínez-Ferrero, A. Viterisi and E. Palomares, *Chem. Soc. Rev.*, 2011, **40**, 1635–1646.
- F. De Angelis, S. Fantacci, A. Selloni, M. K. Nazeeruddin and M. Grätzel, *J. Am. Chem. Soc.*, 2007, **129**, 14156–14157.
- M. K. Nazeeruddin, A. Kay, E. Miiller, P. Liska, N. Vlachopoulos, M. Grätzel, C.- Lausanne and R. April, 1993, **115**, 6382–6390.

- 10 M. K. Nazeeruddin, F. De Angelis, S. Fantacci, A. Selloni, G. Viscardi, P. Liska, S. Ito, B. Takeru and M. Grätzel, *J. Am. Chem. Soc.*, 2005, **127**, 16835–16847.
- 11 S. R. Jang, J. H. Yum, C. Klein, K. J. Kim, P. Wagner, D. Officer, M. Gratzel and M. K. Nazeeruddin, *J. Phys. Chem. C*, 2009, **113**, 1998–2003.
- 12 S. M. Zakeeruddin, K. Nazeeruddin, R. Humphry-Baker, P. Pechy, P. Quagliotto, C. Barolo, G. Viscardi and M. Gratzel, *Langmuir*, 2002, **18**, 952–954.
- 13 D. Kuang, S. Ito, B. Wenger, C. Klein, J.-E. Moser, R. Humphry-Baker, S. M. Zakeeruddin and M. Grätzel, *J. Am. Chem. Soc.*, 2006, **128**, 4146–4154.
- 14 N. Blouin, A. Michaud, D. Gendron, S. Wakim, E. Blair, R. Neagu-Plesu, M. Belletête, G. Durocher, Y. Tao and M. Leclerc, *J. Am. Chem. Soc.*, 2008, **130**, 732–742.
- 15 J. Feng, Y. Jiao, W. Ma, M. K. Nazeeruddin, M. Grätzel and S. Meng, *J. Phys. Chem. C*, 2013, **117**, 3772–3778.
- 16 A. N. Sokolov, S. Atahan-Evrenk, R. Mondal, H. B. Akkerman, R. S. Sánchez-Carrera, S. Granados-Focil, J. Schrier, S. C. B. Mannsfeld, A. P. Zoombelt, Z. Bao and A. Aspuru-Guzik, *Nat. Commun.*, 2011, **2**, 437.
- 17 K. C. D. Robson, B. D. Koivisto, A. Yella, B. Spornova, M. K. Nazeeruddin, T. Baumgartner, M. Grätzel and C. P. Berlinguette, *Inorg. Chem.*, 2011, **50**, 5494–5508.
- 18 T. Le, V. C. Epa, F. R. Burden and D. a Winkler, *Chem. Rev.*, 2012, **112**, 2889–2919.
- 19 D. H. Omkvist, S. B. Larsen, C. U. Nielsen, B. Steffansen, L. Olsen, F. S. Jørgensen and B. Brodin, *AAPS J.*, 2010, **12**, 385–96.
- 20 P. Crivori, G. Cruciani, P. a Carrupt and B. Testa, *J. Med. Chem.*, 2000, **43**, 2204–2216.
- 21 L. H. Alifrangis, I. T. Christensen, a Berglund, M. Sandberg, L. Hovgaard and S. Frokjaer, *J. Med. Chem.*, 2000, **43**, 103–13.
- 22 V. Venkatraman, P.-O. Åstrand and B. K. Alsberg, *J. Comput. Chem.*, 2014, **35**, 214–26.
- 23 E. Maggio, N. Martsinovich and A. Troisi, *J. Phys. Chem. C*, 2012, **116**, 7638–7649.
- 24 D. Pugliese, F. Bella, V. Cauda, A. Lamberti, A. Sacco, E. Tresso and S. Bianco, *ACS Appl. Mater. Interfaces*, 2013, **5**, 11288–11295.
- 25 H. G. Vogel, J. Maas, F. J. Hock and D. Mayer, *Drug Discovery and Evaluation: Safety and Pharmacokinetic Assays*, Springer Berlin Heidelberg, Berlin, Heidelberg, 2013.
- 26 G. Cruciani, M. Pastor and W. Guba, *Eur. J. Pharm. Sci.*, 2000, **11 Suppl 2**, S29–39.
- 27 G. Cruciani, P. Crivori, P.-A. Carrupt and B. Testa, *J. Mol. Struct.: THEOCHEM*, 2000, **503**, 17–30.
- 28 M. J. Frisch, G. W. Trucks, H. B. Schlegel, G. E. Scuseria, M. A. Robb, J. R. Cheeseman, G. Scalmani, V. Barone, B. Mennucci, G. A. Petersson, H. Nakatsuji, M. Caricato, X. Li, H. P. Hratchian, A. F. Izmaylov, J. Bloino, G. Zheng, J. L. Sonnenberg, M. Hada, M. Ehara, K. Toyota, R. Fukuda, J. Hasegawa, M. Ishida, T. Nakajima, Y. Honda, O. Kitao, H. Nakai, T. Vreven, J. A. Jr. Montgomery, J. E. Peralta, F. Ogliaro, M. Bearpark, J. J. Heyd, E. Brothers, K. N. Kudin, V. N. Staroverov, R. Kobayashi, J. Normand, K. Raghavachari, A. Rendell, J. C. Burant, S. S. Iyengar, J. Tomasi, M. Cossi, N. Rega, M. J. Millam, M. Klene, J. E. Knox, J. B. Cross, V. Bakken, C. Adamo, J. Jaramillo, R. Gomperts, R. E. Stratmann, O. Yazyev, A. J. Austin, R. Cammi, C. Pomelli, J. W. Ochterski, R. L. Martin, K. Morokuma, V. G. Zakrzewski, G. A. Voth, P. Salvador, J. J. Dannenberg, S. Dapprich, A. D. Daniels, Ö. Farkas, J. B. Foresman, J. V. Ortiz, J. Cioslowski and D. J. Fox, *GAUSSIAN 09 (Revision A.02)*, Gaussian Inc., Wallingford, CT, 2009.
- 29 A. D. Becke, *J. Chem. Phys.*, 1993, **98**, 5648–5652.
- 30 W. J. Hehre, R. Ditchfeld and J. A. Pople, *J. Chem. Phys.*, 1972, **56**, 2257–2261.
- 31 M. J. S. Dewar, E. G. Zoebisch and E. F. Healy, *J. Am. Chem. Soc.*, 1985, **107**, 3902–3909.
- 32 B. J. Lynch, P. L. Fast, M. Harris and D. G. Truhlar, *J. Phys. Chem. A.*, 2000, **104**, 4811–4815.
- 33 J. Ridley and M. Zerner, *Theor. Chim. Acta.*, 1973, **32**, 111–134.
- 34 J.-F. Yin, M. Velayudham, D. Bhattacharya, H.-C. Lin and K.-L. Lu, *Coord. Chem. Rev.*, 2012, **256**, 3008–3035.
- 35 S. Wold and M. Sjöström, *Chemom. Intell. Lab. Syst.*, 2001, **58**, 109–130.
- 36 G. Cruciani, M. Baroni, S. Clementi, G. Costantino, D. Riganelli and B. Skagerberg, *J. Chemom.*, 1992, **6**, 335–346.
- 37 N. K.-W. and S. W. I. Eriksson, E. Johansson, *J. Chemom.*, 2002, **16**, 117–118.
- 38 A. Abbotto, C. Barolo, L. Bellotto, F. De Angelis, M. Graetzel, *Chem. Commun. (Camb.)*, 2008, **42**, 5318–5320.
- 39 X. Li, A. Reynal, P. Barnes, R. Humphry-Baker, S. M. Zakeeruddin, F. De Angelis and B. C. O'Regan, *Phys. Chem. Chem. Phys.*, 2012, **14**, 15421–15428.
- 40 C. Dragonetti, L. Falciola, P. Mussini, S. Righetto, D. Roberto, R. Ugo, A. Valore, F. De Angelis, S. Fantacci, A. Sgamellotti, M. Ramon and M. Muccini, *Inorg. Chem.*, 2007, **46**, 8533–8547.
- 41 J. E. Kroeze, N. Hirata, S. Koops, K. Nazeeruddin, L. Schmidt-mende, M. Gra and J. R. Durrant, 2006, 16376–16383.
- 42 L. Schmidt-Mende, J. E. Kroeze, J. R. Durrant, K. Nazeeruddin and M. Gra, *Nano Lett.*, 2005, **5**, 1315–1320.
- 43 C.-Y. Chen, H.-C. Lu, C.-G. Wu, J.-G. Chen and K.-C. Ho, *Adv. Funct. Mater.*, 2007, **17**, 29–36.
- 44 P. Salvadori, G. Marotta, A. Cinti, C. Anselmi, E. Mosconi and F. De Angelis, *J. Phys. Chem. C*, 2013, **117**, 3874–3887.
- 45 K. Fredin, J. Nissfolk, G. Boschloo and A. Hagfeldt, *J. Electroanal. Chem.*, 2007, **609**, 55–60.
- 46 M. Yanagida, T. Yamaguchi, M. Kurashige, K. Hara, R. Katoh, H. Sugihara and H. Arakawa, *Inorg. Chem.*, 2003, **42**, 7921–7931.